Electrochimica Acta 82 (2012) 558–569

Contents lists available at SciVerse ScienceDirect

Electrochimica Acta

journal homepage: www.elsevier.com/locate/electacta

Pt(1 1 1) surface disorder kinetics in perchloric acid solutions and the influence of specific anion adsorption

Ana Mª. Gómez-Marín, Juan M. Feliu*,[1]

Instituto de Electroquímica, Universidad de Alicante, Apt 99, E-03080 Alicante, Spain

ARTICLE INFO

Article history:
Received 9 December 2011
Received in revised form 18 April 2012
Accepted 18 April 2012
Available online 4 May 2012

Keywords:
Pt(1 1 1)
Stepped Pt surfaces
Surface reordering kinetics
Electrochemical surface oxidation
Anion adsorption
Surface oxygenated species

ABSTRACT

A significant number of electro-catalytic reactions take place in a potential region in which the surface of platinum is partly covered by oxygenated species. In this respect, the initial oxidation of Pt surfaces is an important process that could determine the reactivity of this catalyst. The understanding of electrochemical Pt oxidation has been hindered by a lack of surface structural definition. In this work, the electro-oxidation of Pt(1 1 1) electrode in the absence and presence of weak and moderately strong specific anion adsorption, and the subsequent surface modification induced by oxygen adsorption are studied. Two different potential dependences are found for the surface reordering kinetics in perchloric acid solutions, at higher and lower potentials, whereas only one appears on sulphate containing solutions. Additionally, a dual role of sulphate anion is observed: at high sulphate concentrations the protective character of the ordered sulphate adlayer delays surface disordering while small concentrations of sulphate anions increase the rate of surface reordering. Water dissociation is at the origin of the double behaviour in $HClO_4$ and also explains the dual role of sulphate anions. It is concluded that platinum oxidation is a complex process that involves several adsorbed species that appear at increasing potentials. All of these process are influenced by anion adsorption and coexist during the initial stages of Pt(1 1 1) oxidation.

© 2012 Elsevier Ltd. All rights reserved.

1. Introduction

Understanding the structure and composition of metal/electrolyte interfaces in an electrochemical environment and under realistic conditions remains a crucial aspect in various research fields such as surface electrochemistry and corrosion science, *e.g.* see [1] and references therein. In electrocatalysis, the surface oxidation–reduction process at Pt electrodes is one of the most important topics.

The oxide growth at Pt electrodes (α-oxide) has been studied for many years [2–5]. It was recognized from electrochemical evidence that oxidizing and reducing the electrode modifies its initial structure (*i.e.* the Pt atoms move from their original positions). Moreover, it is well known that the surface crystallographic orientation and the electrolyte composition result in a unique interface that gives rise to metal–anion interactions which, consequently, affect the potential at which the oxide growth starts [2]. At the same time, the presence of an oxide film affects the mechanism and kinetics of various redox reactions at the surface [6–9].

In 1980 it was proposed that surface oxidation of Pt(1 1 1) led to surface disordering to understand the changes observed in the voltammogram. This conclusion was supported by an ultrahigh vacuum (UHV) surface sensitive technique as low energy electron diffraction (LEED) measurements by Wagner and Ross [3] and Aberdam et al. [5]. They interpreted the surface modification in terms of formation of random steps and terraces. Later, direct *in situ* images of reordered surfaces were obtained by scanning tunnelling microscopy (STM) [10,11]. These showed that, after a single oxidation–reduction cycle, the surface had plenty of small clusters and isolated Pt adatoms on the terraces; following few cycles the surface showed an unusual "rolling hills" topography. In this situation, the hills are about 5 nm apart, have diameters of 2–3 nm and are 2–3 nm high. Afterwards, *in situ* X-ray reflectivity results for this surface have been interpreted in terms of place-exchange [12]. In this model, surface atoms are lifted from the original topmost close-packed layer, exposing atoms on three different levels. Recently, a quantification of the defects created during the potential cycling of initially well-ordered Pt(1 1 1) and its vicinal surfaces on 0.5 M H_2SO_4 has been reported [13,14].

Despite all these studies, many issues are still unclear, especially concerning to the oxidation mechanism and the nature of the species involved in the process.

Interaction of oxygen with the Pt(1 1 1) surface has been studied intensively during last decade from both theoretical

* Corresponding author. Tel.: +34 965 909 301; fax: +34 965 903 537.
E-mail address: juan.feliu@ua.es (J.M. Feliu).
[1] ISE member.

0013-4686/$ – see front matter © 2012 Elsevier Ltd. All rights reserved.
http://dx.doi.org/10.1016/j.electacta.2012.04.066

and experimental point of view, particularly under UHV conditions. Oxygen atoms can populate a variety of states or phases on Pt(1 1 1), including phases that are intermediate between a dilute chemisorbed layer and the bulk oxide(s) [15,16], which in turn affect the reactivity of the catalytic surface. They arrange to minimize various destabilizing interactions with neighbour oxygen. These destabilizing interactions have electronic and strain components that can either reinforce or oppose one to another, depending the O—O separation [17]. The development and properties of these atomic oxygen layers on Pt(1 1 1) are relatively insensitive to the identity of the gaseous oxidant, at least for temperatures ≥300 K [18]. In addition, by using periodic density functional theory (DFT) calculations, aiming to mimic the electrochemical environment, Fang and Liu have proposed that the water environment only affects marginally the surface phase diagram and the oxygen coupling kinetics on Pt(1 1 1) [19].

Nowadays, it is well established that oxygen atoms bind at fcc hollow sites on Pt(1 1 1) below 0.25 monolayer (ML), and arrange into ordered $p(2 \times 2)$ domains [15,18,20]. At this low coverage, oxygen atoms desorb recombinatively during temperature programmed desorption (TPD) experiments to produce a single broad desorption feature. Above 0.25 ML, the TPD spectra exhibit a second desorption feature, at lower temperature than the previous one, that intensifies as the coverage increases to 0.5 ML [15,18,20,21]. A third desorption feature then becomes evident, again at lower temperature than the second one. This peak primarily intensifies with increasing coverage from 0.5 to 0.75 ML. The formation of the third feature correlates with the disruption of the long range order of the surface. Thus, one can expect that any surface with O coverage greater than 0.5 ML is metastable to the formation of a surface oxide and any coverage that can be considered owe their existence to the kinetic resistance of the Pt(1 1 1) surface to the formation of such an oxide [17]. Usually, it has been proposed that sub-surface oxygen species may be the precursor to the formation of these surface oxides.

In electrochemical environments, it has been suggested that the oxide growth proceeds forming first thin α-PtO_2 or PtO surface oxide at not too high electrode potentials. Further growing results in α-PtO_2 or β-PtO_2 bulk oxide [1]. This α-PtO_2 surface oxide is metastable to surface oxygen at lower oxygen chemical potentials [17]. In this respect, it is clear that the oxidation of Pt(1 1 1) is a complex process including different oxygen states that compete between them: chemisorbed oxygen (O_{ads}), sub-surface oxygen (O_{ss}) and different structures of platinum oxide such as PtO, α-PtO_2 or β-PtO_2 bulk oxide.

Under electrochemical conditions, these processes are further complicated by the additional existence of H_2O_{ads}, OH_{ads}, and its water/OH_{ads} network coexisting on the surface during the initial stages of Pt(1 1 1) oxidation [22], especially considering that the local surface structure and coverage could be more important in affecting the barrier of oxygen coupling surface reactions than the electric fields [19,23]. In addition, all these processes are influenced by anion adsorption. Continuing the research on this subject [13,14,23], the electro-oxidation of Pt(1 1 1) electrode in the absence and presence of weak and moderately strong specific anion adsorption, and the subsequent surface modification induced by oxygen underpotential deposition (UPD) are studied. The results help to shed light for unravelling the nature of the species involved in the process and the mechanism during Pt(1 1 1) surface disorder kinetics, together with understanding the anion adsorption role in the surface reordering. The approach is to relate careful electrochemical experiments with data from DFT calculations and *ex situ* UHV experiments, that could be considered as ideal models, and those obtained by *in situ* STM measurements, that supply detailed local information.

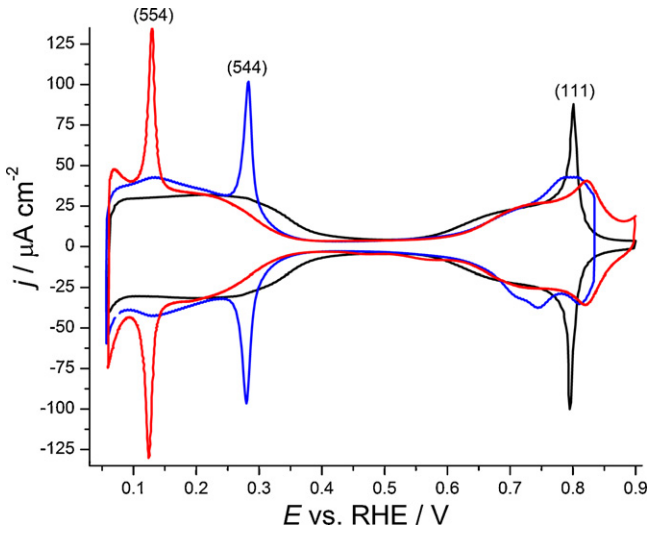

Fig. 1. Stable voltammetric profiles of Pt(1 1 1) (black), Pt(5 5 4) (red), Pt(5 4 4) (blue). (For interpretation of the references to colour in this figure legend, the reader is referred to the web version of this article.)

2. Experimental

Electrodes with (1 1 1) surface orientation or vicinal to this plane were prepared from small Pt beads, approximately 2–3 mm in diameter, by the method described by Clavilier et al. [24]. Experiments were carried out in a two-compartment, three electrode all-glass cell. Prior to each experiment the electrodes were flame annealed, cooled in a hydrogen/argon atmosphere and transferred to the cell protected by a drop of ultra-pure water saturated with these gases. Suprapure grade sulphuric and perchloric acids (Merck) were used to prepare the aqueous solutions in ultrapure water (Purelab Ultra, Elga-Vivendi). All potentials were measured against the Reversible Hydrogen Electrode (RHE) and a flame cleaned Pt wire coil was used as a counter electrode. All voltammetric scans were collected at freshly annealed surfaces, cycled first in the low potential region to verify their quality as well as the cleanliness of the surface. The stability of the voltammetric profiles with time was carefully checked to ensure solution cleanliness [9,10].

Similar to previous work [13,14], our strategy is to characterize and quantify defects by electrochemical means. Since well ordered monatomic stepped electrodes are known to give voltammetric peaks in the low potential region [25–27], the comparison of the characteristic responses of surfaces after oxidation/reduction to these reference data gives information on the amount of defects and their local geometry. The two series of stepped surfaces vicinal to Pt(1 1 1) are denoted Pt(s)[n(1 1 1) × (1 1 1)] ≡ Pt(s)[(n − 1)(1 1 1) × (1 1 0)] and Pt(s)[n(1 1 1) × (1 0 0)]. They are composed of close-packed {1 1 1} terraces, separated at regular intervals by monatomic steps that form micro-facets of {1 1 0} (equivalently denoted {1 1 1} × {1 1 1}) or {1 0 0} orientation. Thus stepped surfaces are characterized by a step orientation, a terrace orientation and a terrace width.

Fig. 1 shows the stable blank voltammetry of Pt(1 1 1), Pt(5 5 4) (or Pt(s)[10(1 1 1) × (1 1 1)] ≡ Pt(s)[9(1 1 1) × (1 1 0)]) and Pt(5 4 4) (or Pt(s)[9(1 1 1) × (1 0 0)]) in 0.1 M perchloric acid. Although their origin is not entirely clear [27,29–31], the sharp peaks seen in the cyclic voltammogram (CV) of the stepped surfaces at 0.13 (for {1 1 0} steps) and 0.28 V *vs.* RHE (for {1 0 0} steps) are very characteristic for steps of these two orientations and they can be related to the eventual formation of defects [13,14,32]. For surfaces with terrace widths larger than a few atoms, individual steps are far away enough from each other to consider that step dipoles interaction is negligible. In this respect, the peak potentials are constant

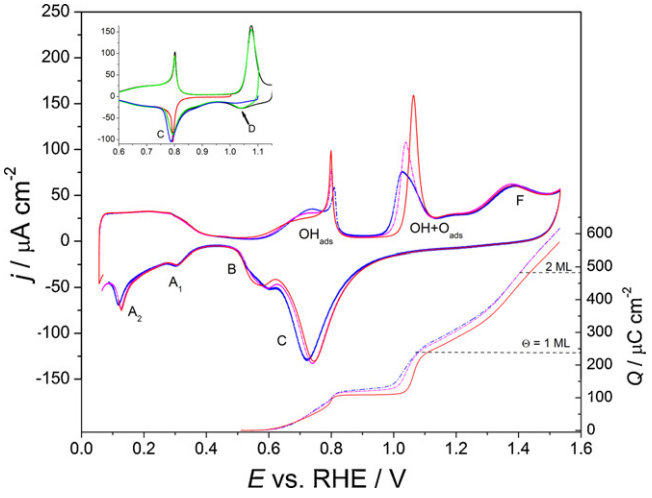

Fig. 2. Cyclic voltammograms (CVs) of Pt(1 1 1) in different aqueous solutions at 50 mV s^{-1} (left *y*-axis), and integral of those curves after double-layer charging correction (right *y*-axis): 0.1 M $HClO_4$ (——), 0.022 M $HClO_4$ (– – –), 0.005 M $HClO_4$ (— • — • —). Inset: detailed view of different upper potential limits on the CV for Pt(1 1 1) in 0.1 M $HClO_4$: 1.15 V (black), 1.1 V (green), 1.0 V (red) and negative-going scan after holding 2 min the potential at 1.1 V (blue). Note that *x* and *y* axes are not the same in the figure and in the inset. (For interpretation of the references to colour in this figure legend, the reader is referred to the web version of this article.)

and the charge densities under these peaks grow linearly with step density, in good agreement with a process where one electron is exchanged per step atom [25,27]. Because of this, blank voltammetry can serve as a tool for quantifying the amount of the two types of step sites present on a surface. At high step densities the shape of the peaks change slightly, and splitting of the corresponding adsorption states occurs, as it appears in the limiting cases of Pt(1 1 0) and Pt(3 1 1) in perchloric acid solutions [27]. This behaviour appears because the steps are no longer isolated from each other, and shows that the local neighbourhood of a defect site affects its adsorption behaviour in the low potential region.

3. Results and discussion

3.1. Electrochemical sub-monolayer oxygen adsorption on Pt(1 1 1) in the absence of specific anion adsorption

An overview of the oxidation behaviour of Pt(1 1 1) in different aqueous solutions is depicted in Fig. 2. The Pt(1 1 1) electrode is electrochemically oxidized in a complex process involving several, pH dependent, oxidation steps, between 0.6 V and the onset of O_2 evolution at about 1.5 V [23]. In this region, at least three oxidation peaks can be identified in perchloric acid solutions. The so-called "butterfly" feature around 0.6–0.8 V is very reversible and usually associated with the anodic adsorption of hydroxide, OH_{ads}, from water [22,28], *via* the following reaction:

$$H_2O + * \rightleftarrows OH_{ads} + H^+ + e^- \quad (1)$$

Its complex shape (see Fig. 2) has been interpreted either as random adsorption followed by a disorder–order phase transition in the adlayer [33], or as the adsorption of OH originating from two types of water [28].

In perchloric acid solutions the second peak, at about 1.06 V in 0.1 M $HClO_4$ at 50 mV s^{-1}, has been attributed to O_{ads} [27,34,35]. The currentless plateau between 0.85 and 1.0 V is considered to be characteristic of well ordered, high quality crystals. With stepped electrodes, there is a significant current in this potential region [23,27]. Some authors have speculated that this plateau could be representative of a kinetic barrier due to a transition between 0.33 ML OH_{ads} and 0.25 ML O_{ads} adsorbed phases, because attaining OH coverages in excess of 0.33 ML appears unlikely [34]. DFT calculations show that at this coverage the structure shows a local minimum in free energy [36]. For an electrochemical interface such simple adlayer picture does not seem probable in light of the complex voltammetric behaviour of Pt [23]. Indeed, reversing the scan at 1.0 V only shows the apparent charging of the double-layer, while at 1.1 V the voltammetric profile is far from reversible (see inset Fig. 2). Nevertheless, as it has been pointed before [23], at 50 mV s^{-1} the irreversibility of the 1.06 V peak does not involve permanent modifications of the surface, because the CV in the low potential region remains stable after this potential excursion. Faster scan rates shift this peak upward toward higher potentials, and can cause surface defects if the potential excursions are beyond 1.15 V.

If the peak at 1.06 V corresponds to a single, ordered oxygen overlayer, its reduction current during the negative-going scan after excursions at higher upper potentials, within this potential range, should show a shift toward positive potentials, because the O coverage is increased, similarly to what is found during UHV studies [15,18,20,21,37] and bearing in mind the marginal role of water environment in the surface phase diagram and the oxygen coupling kinetics on Pt(1 1 1) under electrochemical conditions [19]. Contrarily, after excursions at 1.1 and 1.15 V the CVs do not show any potential shift (see inset Fig. 2). In addition, if the potential is held for 1 or 2 min at 1.1 V, the peaks C and D are slightly shifted toward negative potentials while the D peak decreases (inset Fig. 2). The total charge transferred during this latter experiment is slightly higher than the total charge integrated between 0.55 V and the potential just positive to the second peak at 1.06 V (see bottom Fig. 2). It should be recalled that 0.34 V is the potential of zero total charge for Pt(1 1 1) electrode in 0.1 M perchloric acid electrolyte [38], thus at 0.51 V there is negligible influence of hydrogen adsorption on the integrated charge.

Karlberg and Wahnström have simulated the overlayer formed by dissociation of water on an oxygen covered Pt(1 1 1) surface [39] in very good agreement with the structures seen in STM experiments [40]. They have combined a model potential for the adsorbate–adsorbate interaction among OH_{ads} and adsorbed water molecules, based on DFT calculations, with an Ising type lattice model [39]. Although DFT calculations suggest that OH coverages higher than 0.33 ML cannot be reached [36], it appears that OH coverage as high as 0.5 ML could be possible when the energy contributions from the defects on the adlayer are included [39,41]. In the same way, Anderson et al. have calculated the reversible potentials for water oxidation on Pt(1 1 1) electrodes with different water and OH coverages [42]. Calculations suggest that coverage for OH_{ads} beyond 0.33 ($\frac{1}{3}$) ML can exist only at high electrode potentials, *ca.* 1.30 V, according to the reactions [42]:

$$\tfrac{1}{2}\text{ML } H_2O_{ads} + \tfrac{1}{6}\text{ML } OH_{ads} \rightleftarrows \tfrac{1}{3}\text{ML } OH_{ads} + \tfrac{1}{3}\text{ML } H_2O_{ads} + H^+ + e^- \quad E_{rev} = 0.56\,\text{V} \quad (2)$$

$$\tfrac{1}{3}\text{ML } H_2O_{ads} + \tfrac{1}{3}\text{ML } OH_{ads} \rightleftarrows \tfrac{1}{2}\text{ML } OH_{ads} + \tfrac{1}{6}\text{ML } H_2O_{ads} + H^+ + e^- \quad E_{rev} = 1.30\,\text{V} \quad (3)$$

Here, it is convenient to use fractional stoichiometric numbers in order to highlight the water/OH_{ads} ratio on the adlayer, which is the relevant parameter to describe the strength of the water/OH_{ads} network [42,43]. At the same time, OH_{ads} can be oxidized to O_{ads} even before reaching its highest coverage [43]:

$$\tfrac{1}{3}\text{ML } H_2O_{ads} + \tfrac{1}{3}\text{ML } OH_{ads} \rightleftarrows \tfrac{1}{6}\text{ML } O_{ads} + \tfrac{1}{6}\text{ML } OH_{ads} + \tfrac{1}{3}\text{ML } H_2O_{ads} + H^+ + e^- \quad E_{rev} = 1.12\,\text{V} \quad (4)$$

$$\tfrac{1}{6}\mathrm{ML\ H_2O_{ads}} + \tfrac{1}{2}\mathrm{ML\ OH_{ads}} \rightleftarrows \tfrac{1}{6}\mathrm{ML\ O_{ads}} + \tfrac{1}{3}\mathrm{ML\ OH_{ads}} + \tfrac{1}{6}\mathrm{ML\ H_2O_{ads}} + \mathrm{H^+} + \mathrm{e^-} \quad E_{rev} = 0.8\,\mathrm{V} \tag{5}$$

These works highlight the importance of considering all the possible species involved under electrochemical conditions (water, OH_{ads} and O_{ads}) and multi-scale modelling in order to gain a complete understanding of the fundamental processes observed under electrochemical conditions.

Returning to Fig. 2, the plateau between 0.85 and 1.0 V could be representative of the kinetic barrier of the stable water/OH_{ads} adlayer, formed on the butterfly region, to additional OH adsorption (see Eqs. (2) and (3)). As it can be inferred from Eqs. (2)–(5), if the OH coverage is lower than 0.5 ML its oxidation to O_{ads} cannot occur at low potentials (<0.9 V). However, once the potential is raised (>1.0 V), the OH_{ads} coverage increases and its conversion to O_{ads} is favoured. This new mixed water/OH_{ads}/O_{ads} layer is more stable than the previously built water/OH_{ads} layer with high OH_{ads} coverages (E_{rev} = 0.8 V) and it explains the non-reversible behaviour of the second peak in Fig. 2. It is important to keep in mind that although a process can occur from the thermodynamic point of view, kinetic barriers control its occurrence in the experimental time scale. This situation is reflected in our case during the negative going sweep when the upper potential limit of the CV is higher than 1.0 V (conversion $OH_{ads} \rightleftarrows O_{ads}$).

Within this view, O_{ads} only appears in the second peak of the CV of the Pt(1 1 1) electrode, around 1.06 V, which would correspond to additional OH adsorption followed by its further oxidation, and the surface composition involves water, OH_{ads} and O_{ads}. In this context, the atomic oxygen detected by Wakisaka et al. at 0.9 V, during *ex situ* X-ray photoelectron spectroscopy measurements of the adsorbate structures formed on Pt(1 1 1) in HF solutions, should be due to O_{ads} adsorbed on the defects initially present on the electrode used in the experiment and evidenced in the corresponding CV [22].

At potentials higher than 1.15 V, charge density suggests that all the OH_{ads} on the surface is transformed into O_{ads}, following a complex process that could involve adsorption of O_{ss} as well as Pt oxide formation. This latter species could be formed either by place exchange with O_{ads} or as a result of a chemical reaction between platinum and O_{ads} [15,18,20,37,44–47]. In this potential region, the CVs of Fig. 2 in $HClO_4$ solutions show a shoulder (*ca.* 1.2 V) and a third oxidation peak (F) at about 1.37 V. At potentials higher than peak F, the total adsorption charge reaches two electrons per initial Pt atom and the oxygen UPD process can be considered complete, as it was explained before [23]. The process responsible of the F peak will be discussed in the next section.

3.2. Surface reordering of Pt(1 1 1) in the absence of specific anion adsorption

The electrochemical surface reordering of Pt(1 1 1) electrode in different aqueous solutions has been reported in several papers [3–5,10,11,13,14,27,35,48]. Fig. 3 shows an example of the voltammetry of Pt(1 1 1) during potential cycling up to 1.30 V in 0.1 M $HClO_4$. The stable blank voltammogram after flame annealing between the onset of hydrogen evolution and 1.15 V is given as a reference of the initial state of the electrode. Once the electrode potential is swept beyond 1.15 V (*e.g.* 1.3 V in the figure), the hydrogen adsorption region continuously changes in the subsequent sweeps, witnessing an irreversible topographical change of the electrode surface [25,27]. As shown in Fig. 3, not only the hydrogen adsorption–desorption (E < 0.4 V) but also the surface oxidation–reduction peaks (E > 0.6 V) are modified [3,4,35]. Similarly to the surface disordering in sulphuric acid 0.5 M [13,14], the generated defects display a highly regular evolution of the

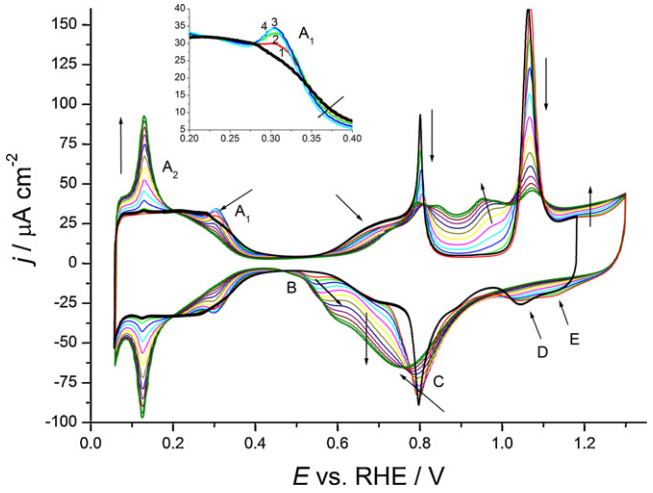

Fig. 3. Voltammetric profiles during the repeated cycling of a Pt(1 1 1) electrode between 0.060 and 1.30 V. Arrows indicate increasing n, the scan rate was 50 mV s^{-1}, electrolyte 0.1 M $HClO_4$. Inset: detailed view in the potential region of the {1 0 0}-type defects. Note that the third and fourth cycles are almost superimposed. During the fifth cycle, the current in that region begins to decrease.

voltammogram and, after a number of cycles, the voltammetric profile reaches a limiting shape indicating that a steady-state distribution and coverage of defects is reached.

In the potential region below 0.4 V, repeated cycling of a Pt(1 1 1) electrode beyond 1.15 V gives rise to two new voltammetric peaks, denoted as A_1 and A_2. These are assumed to correspond to two different types of surface sites, which can be directly identified by comparison with the well-established fingerprint profiles of stepped electrodes (Fig. 1). The A_1 peak initially grows and shifts to lower potentials (≈0.30 V) and finally loses intensity and vanishes (see inset Fig. 3). As this peak potential is close to that observed with ordered {1 0 0}-steps on Pt(s)[n(1 1 1) × (1 0 0)] electrodes, ≈0.28 V (Fig. 1), it can be attributed to {1 0 0}-type defects. It is noteworthy that the charge density under the A_1 peak is significantly lower than that measured in sulphuric acid for the same type of experiments [14]. On the other hand, the state A_2 begins to grow at 0.13 V and can be assigned to {1 1 0}-type defects, following similar arguments. It should be noted that this peak is broader and more asymmetrical than that observed on Pt(s)[n(1 1 1) × (1 1 0)] stepped electrodes. Broader and less symmetric states appear to be related to small, or single site, adsorption states [13,14], thus indicating the disorder of the surface after perturbation.

The voltammetric changes in the region where surface oxidation takes place (E > 0.6 V) are more complex and they resemble some of the voltammetric features of stepped electrodes, especially to those having {1 1 0}-steps [23]. Fig. 4 illustrates the complete oxidation of stepped surfaces vicinal to Pt(1 1 1) for both orientations. It is interesting to note that in the region where peak F occurs on a well ordered Pt(1 1 1), only a broad featureless wave is seen on both stepped and disordered surfaces. This fact suggests that this peak F strongly depends on the surface order. With increasing the number of cycles, both the butterfly feature between 0.6 and 0.8 V and the characteristic peak around 1.06 V decrease. At the same time, the current in the plateau region between 0.85 and 1.0 V increases and after certain number of cycles, two peaks around 0.85 and 0.95 V are defined, similar to the oxidation peaks in the voltammetry of well ordered surfaces having {1 1 0} steps [5,23,27].

Considering the reverse scan, it can be appreciated that during the first cycle, two new peaks appear, named B and E in Fig. 3. The E peak, quite small, decreases and vanishes with each new cycle, while the B peak increases and shifts toward higher potentials, joining C peak when the number of cycles increases. At the

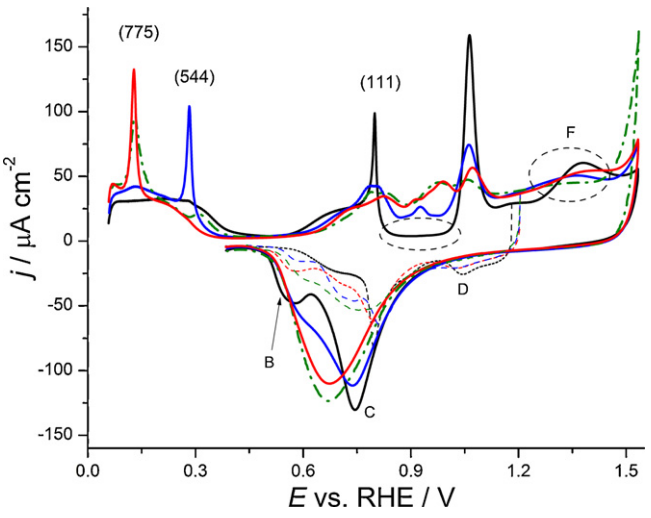

Fig. 4. First oxidation cycles between 0.06 and 1.533 V and between 0.06 and 1.2 V (dashed line) of a Pt(1 1 1) (black), Pt(7 7 5) (red), Pt(5 4 4) (blue) and disordered Pt(1 1 1) (green) electrodes. (For interpretation of the references to colour in this figure legend, the reader is referred to the web version of this article.)

same time, the intensity of D and C peaks decrease with successive cycles, but while D peak vanishes, the C peak broadens and shifts to lower potentials, until the steady state is reached. The increasingly irreversible reduction behaviour related to B and C peaks has been assigned to the low reaction rate of Pt oxide or O_{ads} reduction [10,11,35], while the E peak should correspond to desorption of one particular oxygen state, with lower binding energy, formed when the oxygen coverage on the surface is higher than 0.25 ML (Fig. 2), bearing in mind the oxygen desorption behaviour on TPD studies [15]. The D peak can be due to the desorption either of OH_{ads} remaining on the adlayer or another intermediate oxygen state. In this respect, it disappears at slower scan rates, even when the upper limit is lower than 1.15 V. The exact origin and identity of the B peak is unclear yet, although an attempt to identify the reaction involved is proposed in the next paragraphs.

The formation of defects with preferential {1 1 0}-orientation correlates well with the difference between the kink and step-formation energies for the two step types of Pt(1 1 1) [49–51]. Boisvert and Lewis have given a simple explanation for the origin of this energy difference between the two types of steps in terms of the release of surface stress through relaxation [50]. Employing DFT calculations, it has been shown that the Pt(1 1 1) surface is under significant tensile stress, which can be locally relieved at steps. However, because the atomic configurations are different (albeit slightly) for the two kinds of steps, the relaxation patterns also differ and have different energetics. As a result, the displacements associated to the {1 1 1}-faceted step are larger than for the {1 0 0}-faceted step, *i.e.*, the former can relieve stress more efficiently than the latter, and is thus energetically more favourable. In the same way, STM studies of high temperature oxidation of the Pt(1 1 1) surface have shown the growth of well-ordered PtO_2 nanoclusters with a triangular shape aligned along the [1 $\bar{1}$ 0]direction of the substrate [16].

The development of surface roughness on a Pt(1 1 1) electrode upon potential cycling through the region of surface oxidation and reduction has been also investigated by *in situ* STM studies [10,11,35]. Similar to our results, a steady-state surface structure has been clearly observed after applying a few potential cycles [10,11]. It has been seen that the oxidation of the Pt(1 1 1) does not induce appreciable disordered structures, but the reduction of the oxide layer causes the apparition of islands on the terraces [10,11,35]. Specifically, Wakisaka et al. have reported that nucleation of Pt islands occur during the reduction process after the first surface oxidation, precisely at the final stage of surface reduction around 0.5 V, *i.e.* in the reduction feature that appears as a shoulder in the voltammogram in Fig. 3 (B peak). During repetitive potential cycles, the formation and growth of the Pt islands were found to occur only around 0.5 V in each negative-going potential sweep back from 1.3 V [35].

In order to better understand the nature of B peak and validate if it is the process that necessarily causes the surface disordering on Pt(1 1 1), a experiment was conducted and the results are reported in Fig. 5. First, the Pt(1 1 1) electrode was scanned only once between 0.06 and 1.533 V, a potential just positive to the F peak at 50 mV s^{-1} (see Fig. 2). During the backward scan the lower potential limit was set at 0.7 V and the electrode was cycled between 0.7 and 1.0 V for 1 min. After this ageing perturbation, a CV between 0.06 and 1.0 V was taken. For sake of comparison, a similar cycling experiment was performed but in this case the upper limit in the first scan was set at 1.15 V. In the negative-going scan the lower potential limit was again 0.7 V and the electrode was cycled between 0.7 and 1.15 V during 2 min, then CVs between 0.06 and 1.15 V and 0.06 and 0.9 V were recorded.

As can be appreciated from Fig. 5, while the CV of a well ordered Pt(1 1 1) does not show appreciable changes after the ageing experiment when the upper limit was 1.15 V (arrows, Fig. 5A), when the upper limit in the first sweep was 1.533 V the current recorded around 0.95 V is quite important, even before B peak has occurred (Fig. 5B). It should be recalled that this current is not observed on Pt(1 1 1) but only on its vicinal stepped surfaces (see Fig. 4). This suggests that disordering has already taken place before reaching peak B. In addition, the B peak occurs at the same potential and with the same magnitude than in the case when the ageing experiment is not made (Fig. 5B), provided that the upper limit is high enough. These results imply that, alternatively to what has been suggested by Wakisaka et al. [35], nucleation of Pt islands could not occur strictly at the final stage of the surface reduction around 0.5 V, because there is already surface disordering at 0.7 V. It is probably that, as it has been suggested before [10,11], the beginning of the oxide layer reduction, at around 1.1 V, causes the apparition of islands on the terraces.

In the solid/gas interfaces, the terms O_{ss} and surface oxide have been introduced to distinguish oxygen species with behaviour different from regular O_{ads}. Although the exact location of the different types of oxygen is very difficult to pinpoint, they have been distinguished by their low reactivity and by TPD experiments [6,7,52–55]. Moreover, atomic oxygen can be found in the sub-surface of transition metals during surface reactions in various experimental environments [8,9,16,21,53,55], causing, in some cases, significant changes in their reaction dynamics and catalytic activity. Besides, according to DFT results, surface oxide on Pt(1 1 1) should begin at oxygen coverage higher than 0.5 ML [56]:

$$Pt + O_{ads} \rightleftarrows PtO \quad \theta_{O_{ads}} \geq 0.5 \tag{6}$$

In earlier studies it was suggested that oxide formation occurs through place exchange between platinum and O_{ss} atoms [2,5,12]. During the electro-oxidation of polycrystalline platinum, the initial stages of formation of surface oxide correlate with Pt dissolution, and both oxygen coverage and Pt dissolution depend on the applied potential [57,58] and the sweep rate in cyclic voltammetry experiments [8,9]. In the case of Pt(1 1 1) however, the amount of Pt dissolved is negligible under dynamic oxidation experiments [35], and after polarization at 1.15 V for 24 h, it is only around 0.2 mg cm^{-2} ml^{-1} [59]. In contrast, DFT calculations show that the formation of O_{ss} becomes more favoured, compared to surface oxide, for O_{ads} coverages between 0.5 and 0.75 ML [19,44–46,56] and that OH_{ads} has similar effects on O_{ss} absorption process as those caused by O_{ads} [45].

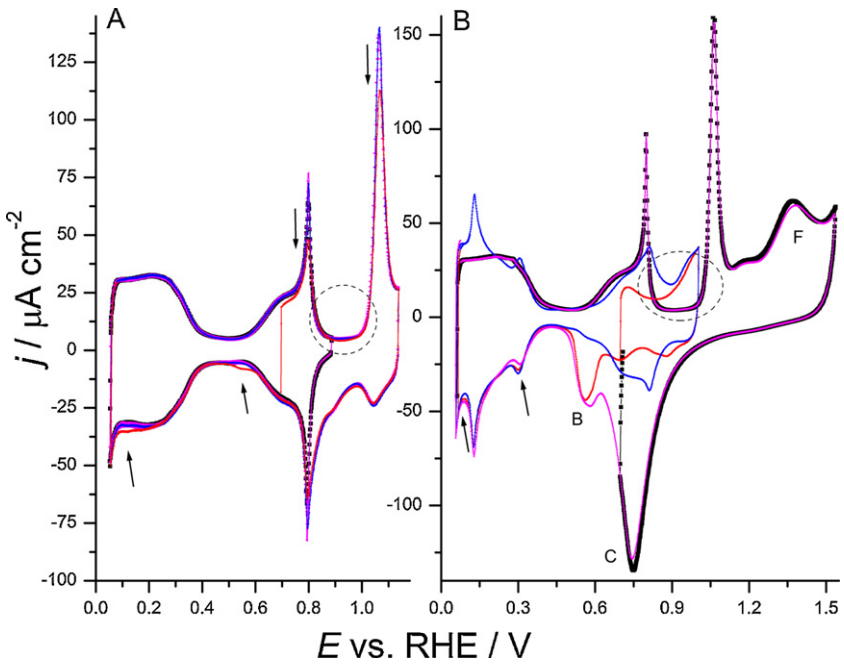

Fig. 5. Current potential profile for a flamed annealed Pt(1 1 1) electrode: one scan between 0.06 and 0.9 V (0.06–1.533 V), A (B) (■). The electrode was continuously cycled 2 min (1 min) between 0.7 and 1.15 V (▼). Afterwards, the electrode was cycled between 0.06 and 1.15 V (0.06–1.0 V) (◆) and 0.06–0.9 V (a flame annealed Pt(1 1 1) electrode, one cycle between 0.06 and 1.533 V) (◀). Arrows A, indicate slight changes in the blank CV. Scan rate 50 mV s^{-1} in 0.1 M $HClO_4$. Note that *x* and *y* axes are not the same in both figures.

Recent STM studies and DFT calculations have suggested a new precursor mechanism to describe the oxidation of Pt(1 1 1) metal surfaces involving Pt oxide chain formation and growth on terraces at moderate oxygen coverages, without O_{ss} participation as precursor [15,56]. Similar one-dimensional PtO_2 growth has been reported at Pt steps [60]. As the coverage increases to 0.75 ML, these chains would form an interconnected network of Y-shaped structures with regions locally resembling a honeycomb. Eventually this structure transforms further into quasi two-dimensional α-PtO_2(0 0 0 1) films [1,56].

In our case, O_{ads} coverage higher than 0.5 ML would imply an electrode potential higher than 1.1 V at 50 mV s^{-1} in 0.1 M $HClO_4$ (see Fig. 2). At this latter potential, *in situ* STM images from Wakisaka et al. [35] show tiny spots covering the whole Pt(1 1 1) surface, attributable to O_{ads}. At higher potentials, the surface becomes bumpy with small height corrugation that is explained by a new place exchange model involving the distortion of the top surface layer of Pt. Nevertheless, considering the *in situ* STM and DFT studies of the initial oxidation of the Pt(1 1 1) surface by Devarajan et al. [15] and Hawkins et al. [56], it can be suggested that the bumpy Pt surface should correspond to initial structures formed during early stages of Pt(1 1 1) oxidation, which do not involve O_{ss} as precursor, following the schema depicted in Eq. (6). These structures would be responsible of the peak F that appears in the CV in $HClO_4$ solutions (see Fig. 2). Similar to UHV studies, the strain relief and long range effects play a large role in the formation and growth of these initial oxide structures.

Although there is already surface disordering before oxide reduction at 0.5 V, it is not possible to see it by *in situ* STM before the peak B has occurred [35]. This fact reveals a correlation between this process and the actual lattice distortion of the surface. Thus, considering previous work on Pt(1 1 0) [54,55] and Pt(1 0 0) [52,53] under UHV environments, and on polycrystalline electrodes in electrochemical conditions [8,9], the B peak can be related to O_{ss} desorption from Pt(1 1 1) according to:

$$Pt(1\,1\,1) + O_{ads} \rightleftarrows Pt(1\,1\,1) - O_{ss} \quad \theta_{(O_{ads}+OH_{ads})} \geq 0.5 \qquad (7)$$

This phenomenon also occurs on stepped surfaces vicinal to Pt(1 1 1) for both orientations, and can be easily appreciated in the reverse scan when the upper potential limit of the CVs is higher than 0.9 V (see Fig. 4). It is important to mention that although this peak develops in a potential region where anion contamination in 0.1 M $HClO_4$ solutions is usually detected [28,61], its origin is related to O_{ss} desorption from the disordered Pt(1 1 1) surface instead of contamination, as it will be shown below (see Section 3.4). In any case, the good charge balance suggests that the latter possibility is scarce in the present case.

Similarly to other reports [8,9], O_{ss} accumulates at $E > 0.85$ V and hinders the OH and O adsorption (see Fig. 5) [59]. Likewise, because O_{ss} is strongly bounded, it desorbs at lower potentials than Pt oxides and even a residual amount can remain at $E < 0.1$ V (see arrows Fig. 5). In agreement with DFT calculations [45], O_{ss} lodges deeper as the total coverage increases making the reverse process more difficult. Besides, this process could be the "unknown slow adsorption process" detected by electrochemical impedance spectroscopy by Bondarenko et al. [34] if not related to surface contamination.

Constant potential and holding experiments (data not shown) suggest that the surface disordering kinetics is faster on cycling experiments, as occurred in sulphuric acid [14]. Conversely, the total charge under the B peak is higher with increasing holding time. Furthermore, again similar to the behaviour in sulphuric acid solutions [14], the stability of the {1 0 0}-type defects on these step experiments is higher than on cycling experiments, which can be understood bearing in mind the slow surface diffusion of platinum atoms at low potential [10,11] and considering the preference of the oxygen atoms for the {1 0 0}-steps over the terraces [19,62,63]. Therefore, as mentioned before [14], the step inter-conversion between {1 0 0} and {1 1 0}-type defects requires dynamic conditions involving the entire reduction of platinum atoms (negative-going scans down to 0.1 V) and their further oxidation over 0.9 V, following a similar process to the formation of {1 1 0}-sites to the detriment of the {1 0 0}-step sites on stepped vicinal surfaces of the [0 $\bar{1}$ 1] zone [64].

It is interesting to note that if a Pt(1 1 1) electrode is disordered at slow scan rates the surface disordering rate also becomes slower, even though the coverage of O-containing species at the same potential limit and the total charge under B peak are higher (calculated from the integration of this peak with reasonably chosen baselines). These results suggest that, contrarily to what has been reported [2,12], although O_{ss} can cause surface disordering, it could prevent it in some extent under certain conditions.

As it was mentioned before, while peak F would correspond to the development of initial oxide structures on Pt(1 1 1), which do not involve O_{ss} (Eq. (6)), peak B, also present on the CV of Pt(1 1 1) vicinal surfaces (see Fig. 4), should correspond to the desorption of O_{ss}. In this scenario, during the initial stages of Pt(1 1 1) oxidation several species such O_{ads}, O_{ss}, initial Pt oxide structures and final surface–oxide phases may coexist depending on the electrode potential and total surface coverage. The fact that Pt(1 1 1) and its vicinal surfaces may contain significant amounts of O_{ss} has not been considered before, and it would imply a whole new paradigm for some electro-oxidation reactions. In this framework, Danilov et al. [7] and Savinova et al. [6] have shown a direct correlation between the concentration of O_{ss} and the copper UPD rate, during copper electro-crystallization studies on polycrystalline platinum both in perchloric and sulphuric acid solutions.

3.3. Potential dependence of the surface disordering rate in the absence of specific anion adsorption

As it has been discussed earlier [3–5,10,11,27,35], the successive changes in the CV when the electrode is repetitively cycled beyond 1.15 V in 0.1 M $HClO_4$, *i.e.*, a continuous growth of the reversible peak at 0.13 V and suppression of the sharp peaks at 0.8 and 1.06 V, suggests an increase of {1 1 0}-type defects and narrowing of the flat {1 1 1} terraces, respectively, on the Pt(1 1 1) electrode [27]. After extensive cycling to high upper potential limit, E_{ox}, the voltammetric profile resembles that of an "activated" polycrystalline electrode (although the peak at 0.27 V is notably absent) [2], illustrating that activation by potential-cycling, employed in most studies of Pt polycrystalline surfaces, in fact destroys all local order and covers the surface with defects [5,14]. Moreover, as can be seen in Fig. 6B, different E_{ox} in the range 1.29–1.39 V lead to similar stationary voltammetric profiles, although these are reached faster as the upper potential limit, E_{ox}, is increased.

During the first oxidation cycle (a cycle is defined by excursion from 0.5 to E_{ox} followed by the reverse scan to 0.06 V and the subsequent positive scan up to 0.5 V), higher E_{ox} causes higher increases of A_1, A_2, B and C peaks, while D and E peaks decrease faster (see Fig. 6A). The development of the A_{1-2} peaks is better observed in the inset of the lower potential region in Fig. 6A. This result implies that the surface undergoes greater modifications with higher E_{ox}, even though in all cases after several cycles voltammograms attain a stationary profile, markedly different from the initial one.

As it was pointed before [13,14], the surface disordering kinetics after electrochemical oxygen adsorption/desorption cycles can be analysed by monitoring the changes in the decreasing population of {1 1 1}-terrace and the evolution of the {1 0 0}- and {1 1 0}-type defect sites. In the present case, terrace OH population is affected by further O adsorption on defects and the signal for {1 0 0}-type defect sites is quite small. In this way, the easiest determination corresponds to the {1 1 0}-type defect sites and its evolution against the number of cycles for different upper potential limits is depicted in Fig. 7A. All changes are referred to the corresponding initial blank voltammogram and the normalization was made with the maximum {1 1 0}-type defect charge reached at the steady state.

Similarly to previous work [13,14], the evolution of the A_2 charge with the number of cycles for different E_{ox} can be well fitted to sigmoid curves, as the final species of a first order consecutive reaction scheme, representing the defect inter-conversion between {1 0 0}- and {1 1 0}-type defects. The presence of monatomic steps on the electrode surface, even at very low density, slows down the disordering kinetics (Fig. 7B). This observation reinforces the expectation that strain relief plays a large role on the initial Pt-oxide formation and its further surface reordering, which can be locally relieved at steps, as was suggested previously. The overall charge increase between 0.06 and 0.5 V, after the oxidation process has reached its steady state, is *ca.* 40 $\mu C\,cm^{-2}$, owing to the increase of microscopic surface area and the higher hydrogen/platinum atom ratio of the {1 1 0}-type defects, assuming the same ratio as that on {1 1 0}-step sites [25,27]. Subtracting the latter step contribution from the overall charge increase, it gives only a small charge due to surface roughness, *ca.* 17 $\mu C\,cm^{-2}$. As shown in Fig. 6B this charge modification is almost the same, independently of E_{ox}, although the steady state is reached faster as the E_{ox} is increased.

To compare the rates of surface reordering in perchloric and sulphuric acid solutions, the characteristic "time constant" for the oxidation process was estimated [14]. A convenient parameter for describing the rate is the "half-life", $n_{½}$, of the A_2 charge development, defined as the number of cycles necessary for the A_2 state to reach half of its limiting value. The values of $n_{½}$ were estimated employing the data fitting of the experimental results to sigmoid curves (see Fig. 7). When the logarithm of this parameter is plotted as a function of E_{ox} linear dependences are obtained (Fig. 8). These "half-lives" provide direct measures of the overall rates of surface reordering under cycling conditions.

It is clear from Fig. 8A that $n_{½}$, in both 0.1 M $HClO_4$ and 0.5 M H_2SO_4 solutions, show exponential dependences on potential. However, they have slightly different behaviour: in 0.5 M H_2SO_4 only one linear dependence, with a slope of −118 mV, is appreciated. Conversely, two linear regions can be identified in 0.1 M $HClO_4$: a low potential region ($E < 1.32$ V) with a linear slope of −138 mV and a high potential region ($E > 1.32$ V) with a linear slope of −222 mV. Furthermore, half-life values are generally shifted to higher potentials in 0.5 M H_2SO_4. These results demonstrate the protective character of the ordered sulphate adlayer and that specific anion adsorption hides elementary steps of the surface reordering mechanism during the Pt(1 1 1) oxidation. It is important to note that this finding is not a consequence of the pH change. On the contrary, surface disordering in 1 M $HClO_4$ is slightly faster than in 0.1 M $HClO_4$ (see Fig. 7B). A possible explanation about this fact will be given in the next section.

3.4. Effect of specific anion adsorption on the surface disordering rate

Considering the large difference in the surface disordering rate and its potential dependence in perchloric and sulphuric acid media, other higher and lower sulphate concentrations were evaluated. Fig. 9 summarizes the first and last profiles when the Pt(1 1 1) electrode is cycled between 0.06 and 1.38 V in 0.1 M $HClO_4$ with different sulphuric acid additions and in different sulphuric acid solutions. In addition, Fig. 10 describes the evolution of the normalized A_2 peak charge with the number of cycles that the Pt(1 1 1) electrode was cycled between 0.06 and 1.364 V in the sulphuric acid (A) and between 0.06 and 1.38 V in the perchloric + sulphuric acid solutions (B). The logarithm of "half-lives" as function of E_{ox} for these solutions has been already shown in Fig. 8A and B, respectively.

From Figs. 8A and 10A, it is clear that anion adsorption protects the surface and diminishes the terrace damage upon disordering. As expected, higher sulphuric acid concentrations increase and shift toward lower potentials the anion adsorption. However, similarly to what has been found during surface reordering in 0.5 M

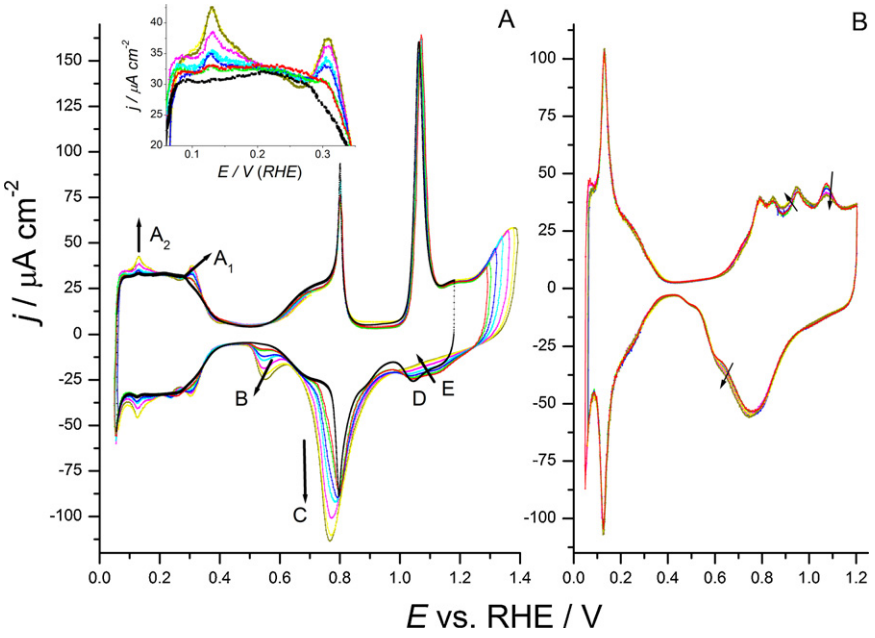

Fig. 6. Initial (A) and steady state (B) voltammetric profiles when cycling a Pt(1 1 1) electrode between 0.060 and different upper potentials, E_{ox}: (■) 1.15 V; (●) 1.29 V; (▲) 1.30 V; (▼) 1.32 V; (◆) 1.34 V; (◀) 1.364 V; (▶) 1.38 V; (⬢) 1.39 V. Cycles are from E_1 = 0.5 V to E_{ox} followed by the reverse scan to 0.06 V and the subsequent positive scan up to 0.5 V. Arrows indicate the effect of increasing potential, the scan rate was 50 mV s^{-1}, electrolyte 0.1 M $HClO_4$. Note that *x* and *y* axes are not the same in both figures. Inset in A shows a detailed view in the potential region between 0.06 and 0.35 V.

H_2SO_4 [14] and shape-controlled nano-particles [65], in all the evaluated solutions the charge balance between usual and unusual states is not fulfilled, *e.g.* the hydrogen and anion adsorption charge ratio is higher than two. As it was pointed out [14,65], the origin of this charge imbalance could be due to the facts that sulphate anion adsorption involves a relative large unit cell, while hydrogen adsorption would simply need a free platinum site, without any particular domain size requirement. The results presented here support the model suggested earlier [14,65], in which two types of {1 1 1} domains would exist: relatively wide hexagonal domains and also narrow domains or isolated sites in which the sulphate network cannot form but could adsorb hydrogen.

As can be seen in Fig. 9B, even small sulphuric acid amounts on the solution suppress the voltammetric current on the CV between *ca.* 0.6 and 0.95 V in 0.1 M $HClO_4$. Considering the CV of stepped surfaces vicinal to Pt(1 1 1), this current can be assigned to adsorption of OH on the terrace and water assisted-step oxidation [23]. Furthermore, while peak C for Pt oxide reduction in $HClO_4$ is almost

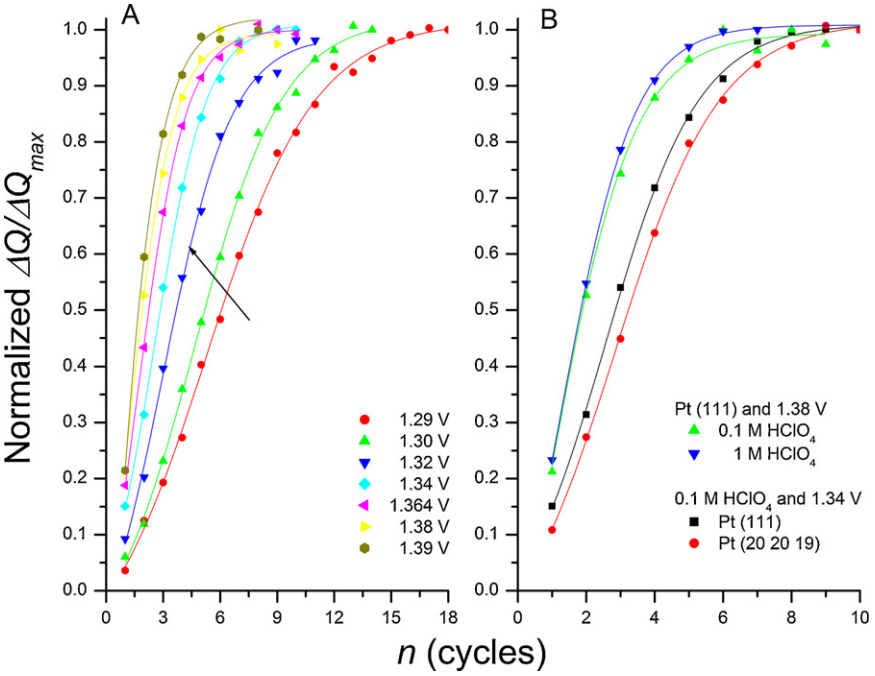

Fig. 7. Evolution of the normalized A_2 peak charge *vs* sweep number, during cycling of a Pt(1 1 1) electrode between 0.06 and different upper potentials, E_{ox}, at 50 mV s^{-1}. (A) 0.1 M $HClO_4$ solutions. The arrow indicates increasing potential. (B) Different electrodes and perchloric acid solutions (see the figure). Solid lines represent best fits to sigmoid curves. Note that *x*-axis is not the same in both figures.

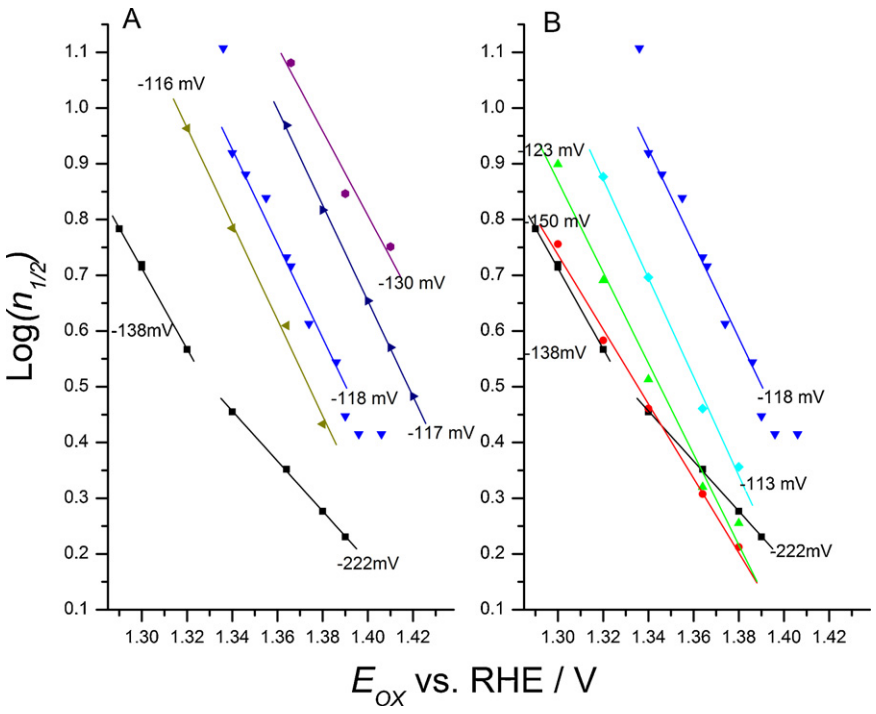

Fig. 8. Summary of the logarithm of the time constants ("Half-life") extracted from cycling experiments, as functions of upper potential, E_{ox} in different sulphate containing solutions A and B. (■) 0.1 M $HClO_4$; (●) 0.1 M $HClO_4$ + 1 × 10^{-4} M H_2SO_4; (▲) 0.1 M $HClO_4$ + 4 × 10^{-3} M H_2SO_4; (◆) 0.1 M $HClO_4$ + 1 × 10^{-2} M H_2SO_4; (◀) 0.05 M H_2SO_4; (▼) 0.5 M H_2SO_4; (▶) 1.0 M H_2SO_4; (⬢) 2.0 M H_2SO_4. Solid lines represent best fits to straight lines.

symmetric (Figs. 2–6), in sulphate containing solutions it becomes increasingly asymmetric as the anion concentration increases. At the same time, the O_{ss} desorption peak, B (Figs. 2–6) shifts slightly toward lower potentials. These results suggest that, similar to that described for polycrystalline platinum [9], desorption of oxygen gives large enough place to the adsorption of anions, which in turn stabilizes residual O_{ss} on the surface. In addition, although the concentration of O_{ss} for the lowest sulphate concentration is higher than in $HClO_4$, it decreases with higher sulphate quantities because of the lower concentration of O-containing species on the electrode surface (see *ca.* 0.5 V, Fig. 9A), at the same upper potential limit. As can be seen, the peak B and the anion desorption peaks appear

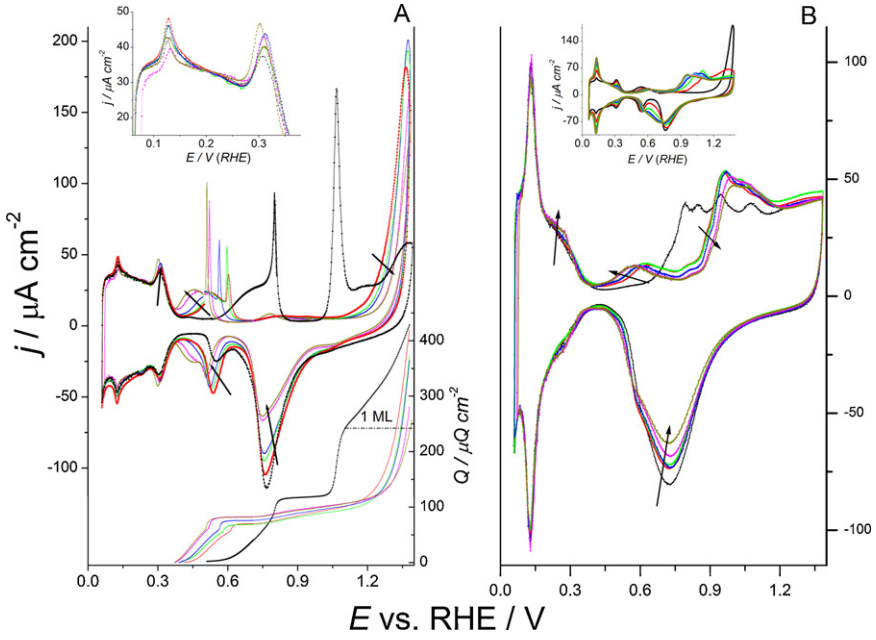

Fig. 9. First (A, left *y*-axis) and last (B) voltammetric profiles when cycling a Pt(1 1 1) electrode between 0.060 and 1.38 V in different sulphate containing solutions, and integral of those curves after double-layer charging correction (A, right *y*-axis). (■) 0.1 M $HClO_4$; (●) 0.1 M $HClO_4$ + 1 × 10^{-4} M H_2SO_4; (▲) 0.1 M $HClO_4$ + 3 × 10^{-4} M H_2SO_4; (▼) 0.1 M $HClO_4$ + 4 × 10^{-3} M H_2SO_4; (◆) 0.1 M $HClO_4$ + 1 × 10^{-2} M H_2SO_4; (◀) 0.05 M H_2SO_4. Arrows indicate increasing sulphate concentrations; the scan rate was 50 mV s^{-1}. Inset A: detailed view in the potential region between 0.25 and 0.38 V. Inset B: voltammetric profiles during the repeated cycling of a Pt(1 1 1) electrode between 0.060 and 1.38 V in 0.1 M $HClO_4$ + 1 × 10^{-4} M H_2SO_4. Note that *y*-axis is not the same in both figures.

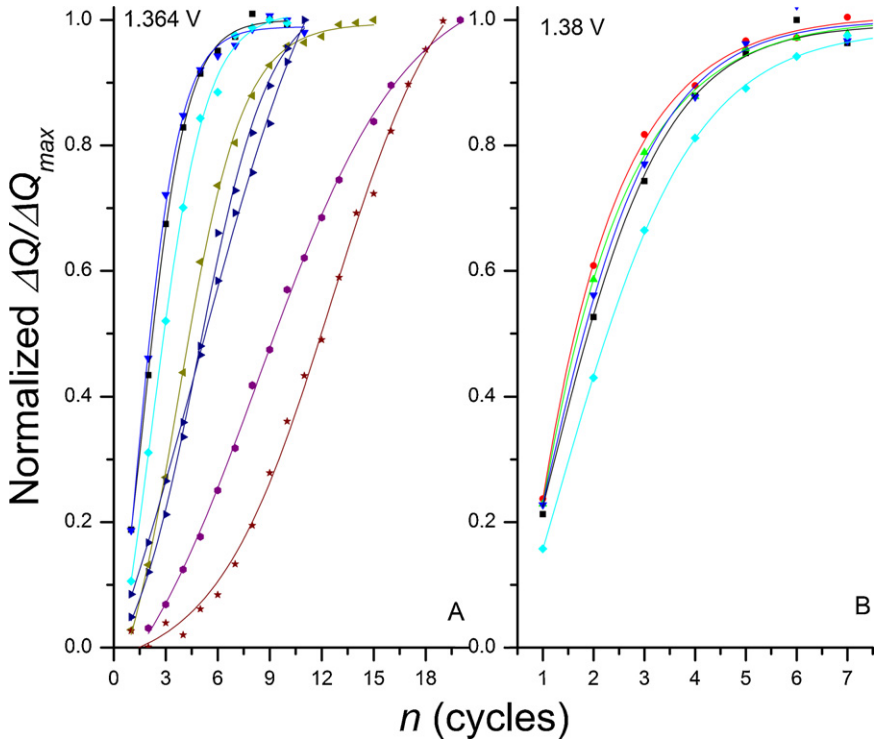

Fig. 10. Evolution of normalized the A_2 peak charge with sweep number, during for cycling of a Pt(1 1 1) electrode in different sulphate containing solutions. E_{ox} = 1.364 V (A); E_{ox} = 1.38 V (B). (■) 0.1 M $HClO_4$; (●) 0.1 M $HClO_4$ + 1 × 10^{-4} M H_2SO_4; (▲) 0.1 M $HClO_4$ + 3 × 10^{-4} M H_2SO_4; (▼) 0.1 M $HClO_4$ + 4 × 10^{-3} M H_2SO_4; (◆) 0.1 M $HClO_4$ + 1 × 10^{-2} M H_2SO_4; (◀) 0.05 M H_2SO_4; (▶) 0.5 M H_2SO_4; (⬢) 1.0 M H_2SO_4; (★) 2.0 M H_2SO_4. Scan rate 50 mV s^{-1}. Solid lines represent best fits to sigmoid curves. Note that *x*-axis is not the same in both figures.

together in the CVs from sulphate containing solutions, which rules out sulphate contamination at the origin of peak B and supports its assignment to O_{ss} discussed before.

The evolution of the A_{1-2} peaks in the solutions with different amount of sulphate anions shows a mixed behaviour (see inset Fig. 9A): while the A_1 peak is higher than in 0.1 M $HClO_4$ with the greatest sulphate quantities, the A_2 peak is higher than in perchloric acid for the lowest sulphate concentrations but it becomes lower for sulphate amounts higher than 0.01 M. It is noteworthy that only for sulphate concentrations higher than 0.05 M, the zone for the {1 0 0}-type defects shows a splitting on two peaks, similar to what is found in 0.5 M H_2SO_4. In the case of 1 M H_2SO_4 solution, neither A_1 nor A_2 peaks are seen on the inset of Fig. 9A because the surface perturbation is very mild for this E_{ox}. It should be mentioned that those peaks are seen at higher E_{ox}, including more than one state in the {1 0 0}-type defect zone, as it was reported before [9,10].

The voltammetric results point out the specific anion adsorption influence on the appearance and stability of the intermediate states in the zone of {1 0 0}-type defects at high sulphate concentrations, and highlight a weakening of its protective role when concentration decreases, exhibiting an opposite behaviour for the smallest quantities of sulphate and highest E_{ox} potentials. Apparently, the presence of small amounts of sulphate anions makes faster the surface reordering kinetics at higher E_{ox} (see Figs. 8B and 10B). In this case, anion adsorption is able to disturb the water network in perchloric acid but has not enough concentration to build a strong sulphate network.

The origin of the dual role of sulphate anions can be understood considering the CV during the first cycle of the surface disordering in each case. As can be appreciated in Fig. 9A, a wide and high current peak appears at higher potentials in solutions with low sulphate anion concentration. This peak also appears in solutions with greater sulphate amounts but it is shifted toward higher potentials and it corresponds to several processes, including those at the peak F identified before (see Fig. 2). The relation between this peak, the sulphate amount and the surface disordering kinetics evidences its role on the surface reordering of Pt(1 1 1) in acidic media. Moreover, on the CV for both stepped and completely disordered surfaces only a wide plateau is seen in the potential region where peak F occurs in perchloric acid (see Figs. 3 and 4). Additionally, after the replacement of adsorbed sulphate by oxygen-containing species, the number of cycles necessary for the A_2 state to reach its limiting value is the same for all E_{ox} provided that the same total charge is transferred during the first oxidative cycle.

An oversimplified microscopic model of the growth of thin anodic oxide film on Pt was proposed by Harrington [66]. According to this model, the rate determining step (RDS) during Pt oxidation process is the migration of a Pt atom from the metal lattice to become a Pt(II) species. Then, Pt(II) species can rapidly diffuse across the surface:

$$\mathrm{Pt(site\,1)} + \mathrm{H_2O_{ads}} \rightleftarrows \mathrm{PtO(site\,2)} + 2\mathrm{H^+} + 2\mathrm{e^-} \quad (8)$$

$$\mathrm{PtO(site\,2)} \overset{k_{O_{diff}}}{\longleftrightarrow} \mathrm{PtO(site\,3)} \quad (9)$$

For cyclic voltammetry, this model predicts a high oxidation peak on the first cycle, followed by a plateau in the behaviour for subsequent cycles, very similar to our experimental results in the presence of sulphate anions for E_{ox} just positive of the F peak (see inset Fig. 9B). However, as can be appreciated from Fig. 8, the slope of the logarithm of $n_{½}$ as a function of E_{ox} in all these cases is close to −118 mV, a typical value of Tafel slopes for simple electrochemical reactions where the first transfer step is the RDS. These findings suggest that, although the peak F might represent the direct formation of Pt(1 1 1) oxide from water, it probably occurs through sequential water oxidation, and oxidation of OH_{ads}

would be the RDS of the mechanism, considering the reversibility of OH_{ads} already formed:

$$PtOH_{ads} \rightleftarrows PtO + H^+ + e^- \quad (10)$$

In this assumption the electrode material would be $PtOH_{ads}$ instead of Pt. The difference between the first and subsequent cycles arrives because the reaction is very difficult on the initial defect-free surface as atoms must be pulled from particularly stable, albeit strained, terrace sites. On the second cycle, the surface has been roughened and higher energy sites such as step and kink sites provide an easier oxidation route [66].

Although the representative parameter, $n_{½}$, is not a fundamental rate constant, it describes the effective overall structural changes of Pt(1 1 1) during voltammetric cycling to high potentials. The deterministic behaviour of this process makes that the slope of the logarithm of $n_{½}$ as a function of E_{ox} equal or close to the Tafel slope of the process [67,68]. For this reason, the values extracted from Fig. 8 can give us an idea about the mechanism of Pt(1 1 1) disordering. Following the model proposed by Harrington [66], Pt oxide formation is a two step process involving an electron transfer (ET) step (Eq. (10)) followed by a diffusion step (Eq. (9)).

In perchloric acid solutions, ET is faster than in the case of solutions containing sulphate anions (see lower potentials in Fig. 8) because O_{ads} is formed at lower potentials through water dissociation on Pt(1 1 1). However, at the same time Pt(II) diffusion should be slightly slower due to the higher amount of O-containing species on the surface (see bottom, Fig. 9A). At higher E_{ox}, the ET is increasingly faster and the diffusion step begins to be the RDS and consequently the Tafel slope increases. In the case of sulphate containing solutions, while the rate of the ET decreases as anion concentration increases, the diffusion process slightly increases. Thus, at low concentrations it can occur that the rate of surface disordering at high potentials is higher than in the case when sulphate anion is absent. Water dissociation is at the origin of the double slope observed in $HClO_4$ (Fig. 8) and also explains the dual role of sulphate anions.

The inclusion of the role of the surface diffusion into the model can also account for the slower surface disordering rate at slower scan rates, together with the presence of O_{ss}, and it is likely that both processes occur simultaneously. On the other hand, it can also explain why Wakisaka et al. [35], only saw a bumpy surface with small height corrugations, taking into account that Pt(II)O might be considered invisible for STM observations due to its rapid diffusion and/or exchange reaction between Pt(II)O and Pt on the lattice.

4. Conclusions

The electro-oxidation of Pt(1 1 1) electrodes, in the absence and presence of weak and moderately strong specific anion adsorption, and the subsequent surface modification induced by oxygen adsorption are studied by employing the voltammetric responses of oxidatively treated Pt(1 1 1) electrode and its vicinal surfaces.

During the initial stages of Pt(1 1 1) oxidation under electrochemical conditions, several species can be considered such as OH adsorbed, chemisorbed oxygen, sub-surface oxygen, initial Pt oxide structures and surface-oxide phases. These species, in addition to water and adsorbed anions, in the case of specifically adsorbing electrolytes, coexist on the surface and their existence strongly depends on the electrode potential and total surface coverage.

In the surface disordering experiments in perchloric acid solutions, the hydrogen adsorption region develops two adsorption states, labelled A_1 and A_2, after continuous oxidation and reduction of the well ordered Pt(1 1 1) electrode. These states can be assigned to two different surface {1 0 0}- and {1 1 0}-type defects, respectively. Similar to 0.5 M H_2SO_4, while the latter state grows following sigmoid kinetics, the former initially increase and afterwards decreases till disappear completely. This analogous behaviour between perchloric and sulphate containing solutions allows to employ the charge under the A_2 peak to measure the overall rate of surface reordering under cycling conditions and compare between the different solutions. The changes in the CVs in the region where surface oxidation takes place ($E > 0.6$ V) are more complex, and they resemble some of the voltammetric features of stepped electrodes, especially to those having {1 1 0}-steps.

Sulphate anions play a dual role during the surface disordering process: at high sulphate concentrations, anion adsorption slows down the rate of surface reordering while at small sulphate amount and high E_{ox} the reordering rate is higher than that measured in pure $HClO_4$. This dual role, jointly with the two different potential dependences for the surface reordering kinetics in perchloric acid solutions, at higher and lower potentials, compared to only one on sulphate containing solutions are explained considering the role of water dissociation during the oxidation process.

Acknowledgments

This study has been carried out in the framework of the European Commission FP7 Initial Training Network "ELCAT", Grant Agreement No. 214936-2. Support from the Spanish MICYNN though project CTQ2010-16271 and GV through PROMETEO/2009/045 (FEDER) are greatly acknowledged.

References

[1] T. Jacob, Journal of Electroanalytical Chemistry 607 (2007) 158.
[2] B.E. Conway, Progress in Surface Science 49 (1995) 331.
[3] F.T. Wagner, P.N. Ross Jr., Journal of Electroanalytical Chemistry and Interfacial Electrochemistry 250 (1988) 301.
[4] N. Furuya, M. Shibata, Journal of Electroanalytical Chemistry 467 (1999) 85.
[5] D. Aberdam, R. Durand, R. Faure, F. El-Omar, Surface Science 171 (1986) 303.
[6] D.V. Savinova, E.B. Molodkina, A.I. Danilov, Y.M. Polukarov, Russian Journal of Electrochemistry 40 (2004) 687.
[7] A.I. Danilov, E.B. Molodkina, Y.M. Polukarov, Russian Journal of Electrochemistry 40 (2004) 597.
[8] D.V. Savinova, E.B. Molodkina, A.I. Danilov, Y.M. Polukarov, Russian Journal of Electrochemistry 40 (2004) 683.
[9] A.I. Danilov, E.B. Molodkina, Y.M. Polukarov, Russian Journal of Electrochemistry 40 (2004) 585.
[10] K. Itaya, S. Sugawara, K. Sashikata, N. Furuya, Journal of Vacuum Science and Technology A 8 (1990) 515.
[11] K. Sashikata, N. Furuya, K. Itaya, Journal of Vacuum Science and Technology B 9 (1991) 457.
[12] H. You, D.J. Zurawski, Z. Nagy, R.M. Yonco, Journal of Chemical Physics 100 (1994) 4699.
[13] A. Björling, E. Ahlberg, J.M. Feliu, Electrochemistry Communications 12 (2010) 359.
[14] A. Björling, J.M. Feliu, Journal of Electroanalytical Chemistry 662 (2011) 17.
[15] S.P. Devarajan, J.A. Hinojosa, J.F. Weaver, Surface Science 602 (2008) 3116.
[16] S.A. Krasnikov, S. Murphy, N. Berdunov, A.P. McCoy, K. Radican, I.V. Shvets, Nanotechnology 21 (2010) 335301.
[17] R.B. Getman, Y. Xu, W.F. Schneider, Journal of Physical Chemistry C 112 (2008) 9559.
[18] J.F. Weaver, J.J. Chen, A.L. Gerrard, Surface Science 592 (2005) 83.
[19] Y.H. Fang, Z.P. Liu, Journal of Physical Chemistry C 113 (2009) 9765.
[20] D.H. Parker, M.E. Bartram, B.E. Koel, Surface Science 217 (1989) 489.
[21] C.R. Parkinson, M. Walker, C.F. McConville, Surface Science 545 (2003) 19.
[22] M. Wakisaka, H. Suzuki, S. Mitsui, H. Uchida, M. Watanabe, Langmuir 25 (2009) 1897.
[23] A. Björling, E. Herrero, J.M. Feliu, Journal of Physical Chemistry C 115 (2011) 15509.
[24] J. Clavilier, D. Armand, S. Sun, M. Petit, Journal of Electroanalytical Chemistry 205 (1986) 267.
[25] J. Clavilier, K. El Achi, A. Rodes, Chemical Physics 141 (1990) 1.
[26] G.A. Attard, O. Hazzazi, P.B. Wells, V. Climent, E. Herrero, J.M. Feliu, Journal of Electroanalytical Chemistry 568 (2004) 329.
[27] J. Clavilier, A. Rodes, K. El Achi, M.A. Zamakhchari, Journal de Chimie Physique 88 (1991) 1291.
[28] A. Berná, V. Climent, J.M. Feliu, Electrochemistry Communications 9 (2007) 2789.
[29] M.T. Koper, J.J. Lukkien, N.P. Lebedeva, J.M. Feliu, R.A. van Santen, Surface Science 478 (2001) L339.

[30] N. García-Araez, J.J. Lukkien, M.T. Koper, J.M. Feliu, Journal of Electroanalytical Chemistry 588 (2006) 1.
[31] M.T.M. Koper, Faraday Discussions 140 (2008) 11.
[32] J. Solla-Gullón, P. Rodríguez, E. Herrero, A. Aldaz, J.M. Feliu, Physical Chemistry Chemical Physics 10 (2008) 1359.
[33] M.T.M. Koper, J.J. Lukkien, Journal of Electroanalytical Chemistry 485 (2000) 161.
[34] A.S. Bondarenko, I.E.L. Stephens, H.A. Hansen, F.J. Pérez-Alonso, V. Tripkovic, T.P. Johansson, J. Rossmeisl, J.K. Nørskov, I. Chorkendorff, Langmuir 27 (2011) 2058.
[35] M. Wakisaka, S. Asizawa, H. Uchida, M. Watanabe, Physical Chemistry Chemical Physics 12 (2010) 4184.
[36] V. Tripkovic, E. Skulason, S. Siahrostami, J.K. Nørskov, J. Rossmeisl, Electrochimica Acta 55 (2010) 7975.
[37] N.A. Saliba, Y.L. Tsai, C. Panja, B.E. Koel, Surface Science 419 (1999) 79.
[38] V. Climent, N. García-Araez, E. Herrero, J. Feliu, Russian Journal of Electrochemistry 42 (2006) 1145.
[39] G.S. Karlberg, G. Wahnström, Physical Review Letters 92 (2004) 136103.
[40] K. Bedürftig, S. Völkening, Y. Wang, J. Wintterlin, K. Jacobi, G. Ertl, Journal of Chemical Physics 111 (1999) 11147.
[41] G.S. Karlberg, F.E. Olsson, M. Persson, G. Wahnström, Journal of Chemical Physics 119 (2003) 4865.
[42] F. Tian, R. Jinnouchi, A.B. Anderson, Journal of Physical Chemistry C 113 (2009) 17484.
[43] F. Tian, A.B. Anderson, Journal of Physical Chemistry C 115 (2011) 4076.
[44] Z. Gu, P.B. Balbuena, Journal of Physical Chemistry C 111 (2007) 9877.
[45] Z. Gu, P.B. Balbuena, Journal of Physical Chemistry C 111 (2007) 17388.
[46] P. Légaré, Surface Science 580 (2005) 137.
[47] D.I. Jerdev, J. Kim, M. Batzill, B.E. Koel, Surface Science 498 (2002) L91.
[48] A.V. Tripkovic, K.Dj. Popovic, J.D. Lovic, Journal of the Serbian Chemical Society 66 (2001) 825.
[49] P.J. Feibelman, Surface Science 463 (2000) L661.
[50] G. Boisvert, L.J. Lewis, M. Schezer, Physical Review B 57 (1998) 188.
[51] J. Ikonomov, K. Starbova, H. Ibach, M. Giesen, Physical Review B: Condensed Matter and Materials Physics 75 (2007) 245411.
[52] J. Dicke, H.H. Rotermund, J. Lauterbach, Surface Science 454–456 (2000) 352.
[53] N. McMillan, T. Lele, C. Snively, J. Lauterbach, Catalysis Today 105 (2005) 244.
[54] A. von Oertzen, A. Mikhailov, H.H. Rotermund, G. Ertl, Surface Science 350 (1996) 259.
[55] A.V. Walker, B. Klotzer, D.A. King, Journal of Chemical Physics 112 (2000) 8631.
[56] J.M. Hawkins, J.F. Weaver, A. Asthagiri, Physical Review B 79 (2009) 125434.
[57] X.P. Wang, R. Kumar, D.J. Myers, Electrochemical and Solid-State Letters 9 (2006) A225.
[58] R.M. Darling, J.P. Meyers, Journal of the Electrochemical Society 150 (2003) A1523.
[59] V. Komanicky, K.C. Chang, A. Menzel, N.M. Markovic, H. You, X. Wang, D. Myers, Journal of the Electrochemical Society 153 (2006) B446.
[60] J.G. Wang, W.X. Li, M. Borg, J. Gustafson, A. Mikkelsen, T.M. Pedersen, E. Lundgren, J. Weissenrieder, J. Klikovits, M. Schmid, B. Hammer, J.N. Andersen, Physical Review Letters 95 (2005) 256102.
[61] J.M. Feliu, R. Gómez, M.J. Llorca, A. Aldaz, Surface Science 289 (1993) 152.
[62] P.J. Feibelman, S. Esch, T. Michely, Physical Review Letters 77 (1996) 2257.
[63] M.J.T.C. van der Niet, A. den Dunnen, L.B.F. Juurlink, M.T.M. Koper, Angewandte Chemie – International Edition 49 (2010) 6572.
[64] A. Rodes, J. Clavilier, Journal of Electroanalytical Chemistry 34 (1993) 269.
[65] Q.S. Chen, F.J. Vidal-Iglesias, J. Solla-Gullón, S.G. Sun, J.M. Feliu, Chemical Science 3 (2012) 136.
[66] D.A. Harrington, Journal of Electroanalytical Chemistry 420 (1997) 101.
[67] M.T.M. Koper, A.P.J. Jansen, R.A. van Santen, J.J. Lukkien, P.A.J. Hilbers, Journal of Chemical Physics 109 (1998) 6051.
[68] A. Gómez-Marín, J.P. Hernández-Ortíz, M.T.M. Koper, in preparation.